Dissociable Functional Networks of the Human Dentate Nucleus

Jessica A. Bernard[1], Scott J. Peltier[2], Bryan L. Benson[3], Jillian Lee Wiggins[1], Susanne M. Jaeggi[5], Martin Buschkuehl[1,5],
John Jonides[1,4], Christopher S. Monk[1,4] and Rachael D. Seidler[1,3,4]

[1]Department of Psychology, [2]Functional MRI Laboratory, [3]School of Kinesiology, and [4]Neuroscience Program, University
of Michigan, Ann Arbor, MI 48109, USA and [5]University of Maryland at College Park, College Park, MD 20740, USA

Address correspondence to Dr Rachael D. Seidler, 401 Washtenaw Avenue, Ann Arbor, MI 48109-2214, USA. Email: rseidler@umich.edu

The cerebellar dentate nucleus has been reported to project to motor
and prefrontal cortical regions in nonhuman primates from 2 anatomi-
cally distinct areas. However, despite a wealth of human neuroimaging
data implicating the cerebellum in motor and cognitive behaviors, evi-
dence of dissociable motor and cognitive networks comprising the
human dentate is lacking. To investigate the existence of these 2 net-
works in the human brain, we used resting-state functional connec-
tivity magnetic resonance imaging. The resting-state fMRI signal was
extracted from regions of interest in the dorsal and ventral dentate
nucleus. We report a "motor" network involving the dorsal dentate,
anterior regions of the cerebellum, and the precentral gyrus, and a
"cognitive" network involving the ventral dentate, Crus I, and prefron-
tal cortex. The existence of these 2 distinct networks supports the
notion that cerebellar involvement in cognitive tasks is above and
beyond that associated with motor response components.

Keywords: cerebellum, dentate nucleus, MRI, resting state connectivity

Introduction

Numerous studies have implicated the cerebellum as having both motor and cognitive functions (Desmond et al. 2005; Schmahmann et al. 2009; Stoodley and Schmahmann 2009; Strick et al. 2009; Diedrichsen et al. 2010), although its role in cognitive processes continues to be debated (Glickstein and Doron 2008). The cerebellar lobules have topographically segregated connections with motor and prefrontal cortical regions in the nonhuman primate (Kelly and Strick 2003; Middleton and Strick 2001), supporting its potential role in higher-level prefrontal functions. In nonhuman primates, the dorsal and ventral portions of the dentate nucleus have differential connections with the cortex (Dum and Strick 2003). The dorsal dentate projects to the primary motor cortex, the ventral premotor cortex, and the anterior intraparietal area via the ventral posterior lateral nucleus of the thalamus. In contrast, the ventral dentate projects to prefrontal cortical areas via the ventral lateral nucleus of the thalamus (Dum and Strick 2003; Clower et al. 2005). However, whether there are 2 distinct dentate-cortical networks in the human brain remains unknown. While the animal literature indicates separate net-works, it is important to note that the dentate nucleus is much larger in the human brain, primarily because the ventral region specifically is expanded (Leiner et al. 1986). Leiner et al. have also pointed out that the dorsal region of the dentate is anato-mically similar to that in other animals, but the ventral region is quite different, and may be associated with cognitive proces-sing. Thus, while the nonhuman primate literature indicates 2 regions with dissociable cerebello-cortical networks, it is important to investigate the potential existence of these net-works directly in the human brain.

Consistent with the proposal that the human ventral dentate is involved in cognitive function (Leiner et al. 1986), Kim et al. (1994) demonstrated activation in the ventral dentate nucleus during the performance of a cognitive task, using functional magnetic resonance imaging (MRI). This work provided the first indication that a dorsal–ventral dis-tinction may exist in the human brain. More recently, the ana-tomical distinction in the human dentate nucleus has been further studied using neuroimaging (Habas 2010; Küper et al. 2011; Thürling et al. 2011). Ventral regions of the dentate nucleus were activated for performance of cognitive tasks whereas dorsal regions of the dentate were predominantly activated by finger tapping (Küper et al. 2011), though motor task activation was seen in both regions. Thus, while Küper et al.' findings suggest a potential functional dissociation in the human dentate nucleus, whether or not these regions are part of 2 distinct processing networks is unclear.

Resting-state functional connectivity MRI (fcMRI) has emerged as a tool to study networks in the human brain in vivo, demon-strating correlated activity between remote brain regions with known anatomical connections and similar functions (Biswal et al. 1995, 2010). This method allows for the investigation of dissociable dentate networks paralleling work in nonhuman pri-mates (Dum and Strick 2003). While a few studies have used this technique to study functional connectivity between the cerebellar cortex and the cerebral cortex (Habas et al. 2009; Krienen and Buckner 2009; O'Reilly et al. 2010; Buckner et al. 2011), none have taken an anatomically driven approach to determine whether dissociable motor and cognitive networks arise from spatially distinct regions of the human dentate nucleus.

Driven by the indication that there are indeed 2 distinct processing regions in the human dentate nucleus, we used resting-state fcMRI to delineate the cortical networks of the human dorsal and ventral dentate (Fig. 1). This allowed us to investigate whether these regions are involved in distinct motor and cognitive networks. Our hypotheses were guided by the networks previously mapped in the nonhuman primate (Dum and Strick 2003; Kelly and Strick 2003; Akkal et al. 2007). We hypothesized that the dorsal dentate would be part of a network of diverse regions associated with motor performance, including the primary motor and premotor cor-tices (Dum and Strick 2003; Akkal et al. 2007), while the ventral dentate would comprise part of a diverse network in-cluding regions of the prefrontal and parietal cortices (Dum and Strick 2003; Clower et al. 2005). Additionally, we pre-dicted that dorsal dentate fluctuations would be correlated with those of anterior regions of the cerebellum and lobules VIIIa and VIIIb often associated with motor functions, whereas ventral dentate activity would be correlated with posterior lobules often associated with cognitive functions (Schmahmann et al. 2009; Strick et al. 2009).
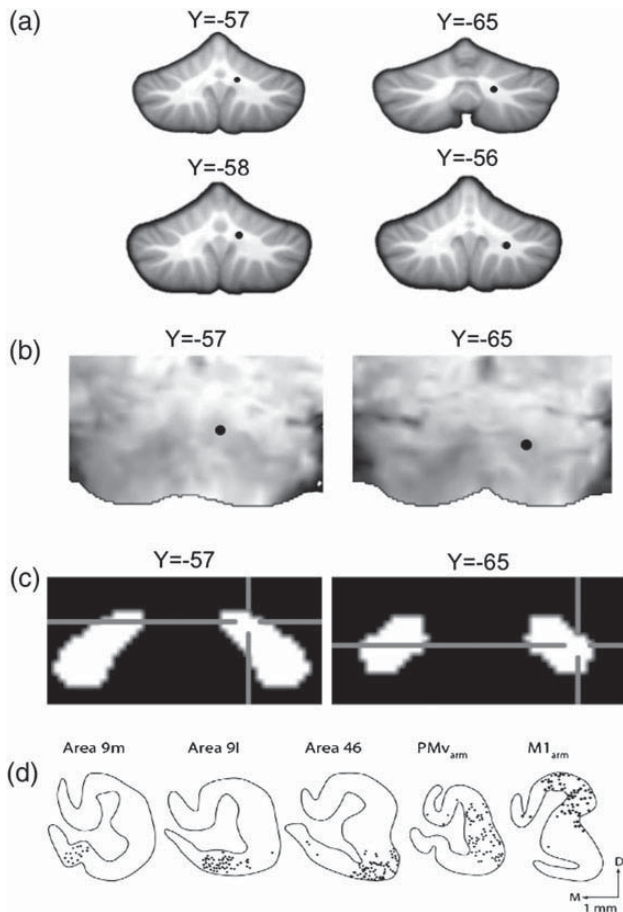
Figure 1. Dentate seed locations. (*a*) Locations of the dorsal (12, −57, −30; top left) and ventral (17, −65, −35; top right) seed regions in the dentate nucleus overlaid on an anatomical image in standardized space. The additional dorsal (10, −58, −31; bottom left) and ventral (20, −56, −37; bottom right) seeds are also presented. The dorsal and ventral seeds were restricted to the dorsal one-third, and bottom half of the dentate nucleus, respectively. (*b*) The seed locations have also been overlaid on a single subject's functional image, in standardized space, to aid visualization. The dark regions are the dentate nuclei (dorsal, left; ventral, right). (*c*) The seed locations denoted on the dentate nucleus from the SUIT atlas (Diedrichsen et al. 2011). Blue-cross hairs indicate the seed location. (*d*) In the monkey dentate, there is a clear topography within the dentate such that the dorsal region projects to the motor cortex, while the ventral region projects to the prefrontal cortex (figure reprinted with permission from Strick et al. 2009).

Materials and Methods

Participants

We recruited 39 participants (age [mean ± SD]: 22.76 ± 2.95 years, 17 females) from the University of Michigan and greater Ann Arbor community. All participants were healthy, with no reported history of neurological or psychiatric disorder, and no contraindications for fMRI scanning. All participants were right handed, based on self-report. Participants signed a consent form approved by the University of Michigan Medical Institutional Review Board. Five participants were excluded from analyses due to motion artifacts, 1 participant was excluded due to insufficient spatial coverage of the cerebellum during MR acquisition, and 2 participants were excluded from analysis due to technical problems during data collection, leaving a total of 31 (15 female) participants.

fMRI Data Acquisition

Functional MRI data were collected with a 3-T GE Signa MR scanner at the University of Michigan. Two structural MR image acquisitions were acquired for each subject. For the structural images, a 3D T_1 axial overlay (TR = 8.9 ms, TE = 1.8 ms, flip angle = 15°, FOV = 260 mm, slice thickness = 1.4 mm, 124 slices; matrix = 256 × 160) was acquired for anatomical localization. To facilitate normalization, a 110-sliced sagittal inversion-prepped T_1-weighted anatomical image using spoiled gradient-recalled acquisition in steady state (SPGR) imaging (flip angle = 15°, FOV = 260 mm, 1.4 mm slice thickness) was acquired.

A single-shot gradient-echo reverse spiral pulse sequence (Glover and Law 2001) was used to collect either 300 (n = 12 participants) or 240 (n = 18 participants) T_2*-weighted BOLD images (TR = 2 s, TE = 30 ms, flip angle = 90°, FOV = 220 mm × 220 mm, voxel size = 3.4 mm × 3.4 mm × 3.2 mm, 40 contiguous axial slices). Our slices were centered so as to cover the entire cerebellum. However, in cases where the head was too large to make this possible, the most inferior portions of the cerebellum were not scanned. A visual fixation cross was presented to the subject using a rear projection visual display. Participants were instructed to keep their eyes focused on the cross, and to not think about anything in particular. There are no clear differences in the oxygen extraction fraction indicative of activation when participants rest with their eyes open or closed (Gusnard and Raichle 2001). Furthermore, studies have indicated close similarity in resting-state networks from scans with both eyes open and closed (Fransson 2005; Van Dijk et al. 2008). Thus, we chose to use an eyes open procedure for the comfort of our participants and to prevent them from falling asleep. Data from 2 experiments using different resting state scan lengths were pooled. The duration of the scan was either 8 or 10 min. A pressure belt was placed on the abdomen of each subject to monitor the respiratory signal. A pulse oximeter was placed on the subject's finger to monitor the cardiac signal. The respiratory, cardiac, and fMRI data collection were synchronized.

fMRI Data Analysis

The functional MRI data were preprocessed as part of the standard processing stream at the University of Michigan. First, K-space outliers in the raw data >2 standard deviations from their mean were replaced with the average of their temporal neighbors. Second, images were reconstructed using field map correction to remove distortions from magnetic field inhomogeneity. Third, physiological variations in the data from the cardiac and respiratory rhythms were removed via regression (Glover et al. 2000). This removed the effects of the first- and second-order harmonics of the externally collected physiological waveforms. Fourth, slice timing differences were corrected using local sinc interpolation (Oppenheim et al. 1999). Lastly, we used MCFLIRT in the fMRIB Software Library (Jenkinson et al. 2002) to perform motion correction (using the 10th image volume as the reference). The 10th slice was chosen as the reference point for 2 main reasons. First, a slice toward the beginning of the scan was preferred so as to minimize the chances of the participant having already moved. Second, using the 10th slice also helped to ensure that the signal was settled. For all participants, head motion was <0.5 mm in the *x*, *y*, or *z* direction.

Structural images were skull-stripped using FSL and we then co-registered the 3D T1 SPGR to the functional images using SPM5 (Wellcome Department of Cognitive Neurology, London, UK; http://www.fil.ion.ucl.ac.uk). The data were then normalized to MNI space using Advanced Normalization Tools (ANTS; Penn Image Computing & Science Lab, http://www.picsl.upenn.edu/ANTS/). The transformation was first applied to the SPGR image, and then the resulting warp vectors were applied to the functional images. Additionally, because of the potential for distortions when normalizing the cerebellum to standard space (Diedrichsen et al. 2009), the cerebellum was normalized separately to a spatially unbiased atlas template (SUIT: Diedrichsen 2006; Diedrichsen et al. 2009) also using ANTS. The warp vectors were then applied to the functional images resulting in normalized whole-brain structural and functional images, and separate normalized cerebellar structural and functional images. Finally, both the cerebellum and whole-brain data were spatially smoothed using a Gaussian kernel of 4-mm full-width half-maximum.

Because of the variable duration of the resting-state scans, only the first 8 min of functional data were used in our analyses. Additionally, the first 5 volumes were discarded to account for scanner equilibration in all participants. The following procedures were used to

generate functional connectivity maps (low-frequency time course correlation maps), and were performed on physiologically corrected data (heart rate and respiration signals were removed). The data were first filtered using a second-order dual-pass band-pass filter to examine the frequency range of interest (0–0.08 Hz) and to exclude higher frequency sources of noise such as heart rate and respiration (Biswal et al. 1995; Peltier et al. 2003). Second, the time course of activity was extracted from the right dentate seed regions (Fig. 1; dorsal and ventral). Several steps were taken with respect to the placement of our dentate seeds. We generated these regions through close examination of figures from the primate literature (Dum and Strick 2003) as well as results from functional MRI studies in humans (Küper et al. 2011), and atlases of the cerebellar nuclei (Dimitrova et al. 2002; Diedrichsen et al. 2011). However, neither of these atlases provides specific demarcations for the dorsal and ventral dentate. Additionally, though the dentate is relatively large ($13 \times 19 \times 14$ mm³; cf. Diedrichsen et al. 2011), in the Dimitrova nuclear atlas (Dimitrova et al. 2002), which served as the primary guide as we placed our seeds, the dentate nucleus extends 13 mm in the medial-lateral direction and 16 mm in the dorsal–ventral direction. Given the spatial resolution of our voxels, this left only a maximum 6 voxels in the medial–lateral direction and 8 voxels in the dorsal–ventral direction. Thus, we restricted the dorsal seed to the most dorsal one-third of the dentate nucleus, and the ventral seed to the ventral half of the dentate nucleus. Given this constraint, we placed the seeds in 2 more extreme locations of the dentate nucleus. The dorsal seed region was centered at 12, −57, −30 (X, Y, Z) and the ventral seed region was centered at 17, −65, −35, both in standardized MNI space. To examine the spatial specificity of the seed selection, in a post hoc analysis, we also placed additional seeds in the dorsal and ventral regions at 10, −58, −30 and 20, −56, −37, respectively. We used the same rule of limiting the dorsal and ventral seeds to the dorsal one-third and ventral half of the nucleus, respectively. Multiple seed locations were placed in the dentate, as there seem to be several distinct regions with projections to the cerebral cortex in the monkey dentate (Dum and Strick 2003). Seeds were also placed in the left dentate, in mirrored locations to the right seeds, in order to investigate the reproducibility of these networks in the left hemisphere. All seed locations were then visually inspected in all participants using their T_2*-weighted functional images in standardized space to ensure that the seeds were located within the dentate nucleus. Because of the small size of the dentate nucleus and its proximity to the cerebellar cortex, single-voxel seeds were used for this analysis to ensure that the signal from the nucleus was not contaminated with that from surrounding cortex, and between the 2 seeds. Furthermore, the seed time courses were extracted from spatially "unsmoothed" data. Third, the time course of the seed was unit normalized to remove differences in variance among subjects. Fourth, the average seed region time course in the filtered data was correlated with all other low-pass filtered voxels in both the cerebellum and the whole-brain functional data (done in 2 separate steps on the spatially smoothed data) to form functional connectivity maps for each dentate seed in each participant. These r-values were converted to z-scores using Fisher's r- to z-transformation. Z-scores from each participant were entered into group-level random-effects analyses, which were carried out using SPM5 (Wellcome Department of Cognitive Neurology, London, UK; http://www.fil.ion.ucl.ac.uk). We evaluated the connectivity maps associated with the dorsal and ventral seeds individually, correcting for multiple comparisons, using an uncorrected $P < 0.00001$ with a voxel extent threshold of at least 100 voxels for both the dorsal and ventral dentate seed networks.

To test the specificity and reproducibility of the dorsal and ventral dissociation, we placed several single-voxel seeds in motor and prefrontal regions of the cortex. This allowed us to investigate dissociable correlations between cortical regions and distinct regions of the dentate nucleus. Seeds were placed in the primary motor cortex (M1), dorsolateral prefrontal cortex (DLPFC), and the frontal pole. The seed locations for M1 (−42, −24, 60) and DLPFC (−42, 16, 36) were taken from a prior resting-state investigation of the motor and cognitive networks of the human cerebellum (Krienen and Buckner 2009). We also included a frontal pole location (0, 62, 4) based on functional

MRI results from Gilbert et al. (2006). The analysis procedure follows that of the dentate seeds with the following exception: the time course was extracted from smoothed data, and was then correlated with unsmoothed data in the cerebellum. This mirrors the analysis procedures of our cerebellar seeds. All results were evaluated using a false discovery rate of $P < 0.001$. A minimum cluster size of 10 was used, given the small size of the dentate nucleus.

Finally, we performed an additional analysis to assess the conjunction of the 2 networks. This allowed us to test the distinctiveness of the dentate networks. A conjunction analysis assesses areas of overlap between 2 contrasts (here, 2 networks). Given that we hypothesize that these are 2 distinct networks, we would expect very little overlap in the conjunction analysis. We created binary masks of the thresholded images for the dorsal and ventral dentate networks. Next, using FSL, the 2 masks were multiplied together. Only regions where there are significant correlations in both of the networks (coded as ones in the binary masks) remain after the multiplication.

Results

Functional Connectivity of the Dorsal and Ventral Dentate

We first identified functional connectivity maps for the dorsal and ventral dentate nucleus in just the cerebellum due to our separate normalization of this structure to the SUIT template (Fig. 2). Our group-level results were similar to the regional motor and cognitive distinctions identified in the nonhuman primate literature (Dum and Strick 2003; Kelly and Strick 2003). That is, the dorsal dentate showed statistically significant connectivity with anterior regions of the cerebellum, in particular, lobules I–IV, V, and VI, though notably there was also a correlation that was on the border between lobule VI and crus I. The ventral dentate meanwhile showed statistically significant connectivity with lobule VI, lobule VIIb (bordering the dentate), vermis VIIIb, and crus II (Table 1). We did not see any correlations between the right dorsal dentate and lobules VIIIa and VIIIb.

We next identified the functional connectivity maps for our 2 dentate seeds with the cortex. The dorsal dentate showed statistically significant connectivity with the primary motor cortex, the premotor cortex, the putamen, and the inferior
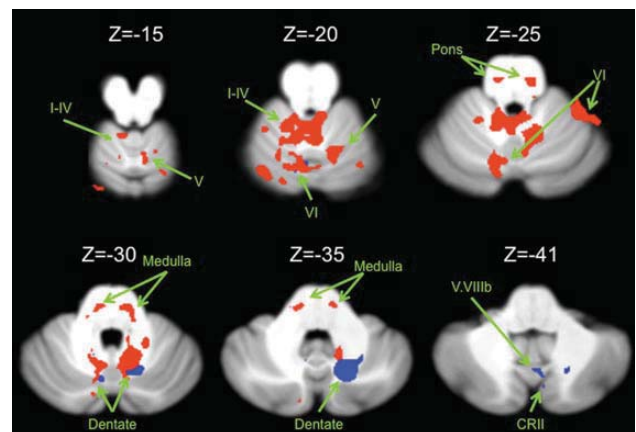
Figure 2. Connectivity maps in the cerebellum. Functional connectivity maps for the dorsal (red) and ventral (blue) dentate in the cerebellum (axial views; both presented at $P < 0.00001$). The dorsal network includes lobules I–IV, V, and VI in the anterior regions of the cerebellum. The ventral network is predominately made up of more posterior regions including crus II, but also extends into lobule VI. Images are oriented such that the right hemisphere is presented on the right. Roman numerals indicate the cerebellar lobules. CRII: crus II.

Seed	Region	MNI coordinates			T-value
		X	Y	Z	
Dorsal dentate	**Dorsal dentate**	**12**	**−58**	**−30**	**29.49**
	Lobules I–IV	6	−42	−21	8.79
	Lobule VI	16	−63	−13	8.14
	Pons	**−7**	**−26**	**−28**	**8.98**
	Medulla	−16	−30	−33	8.95
	Lobule VI/crus I	**44**	**−48**	**−24**	**7.60**
	Lobule VI	37	−42	−23	7.22
	Lobule V	25	−39	−18	5.96
	Pons	**−15**	**−25**	**−4**	**7.50**
	Pons	−9	−32	−2	6.71
	Lobule VI	**29**	**−55**	**−27**	**6.40**
	Lobule VI	23	−62	−27	4.48
Ventral dentate	**Ventral dentate**	**18**	**−65**	**−36**	**27.91**
	Dentate/lobule VIIb	**−7**	**−69**	**−32**	**7.52**
	Dentate nucleus	−11	−55	−32	7.22
	Vermis VIIIb	**4**	**−65**	**−43**	**6.67**
	Crus II	7	−73	−37	5.38
	Lobule VI	**−7**	**−69**	**−21**	**6.55**

Negative x-values indicate locations in the left hemisphere, while positive x-values indicate locations in the right hemisphere. Regions in bold indicate the peak voxel of a cluster. Additional local maxima are presented in standard font.
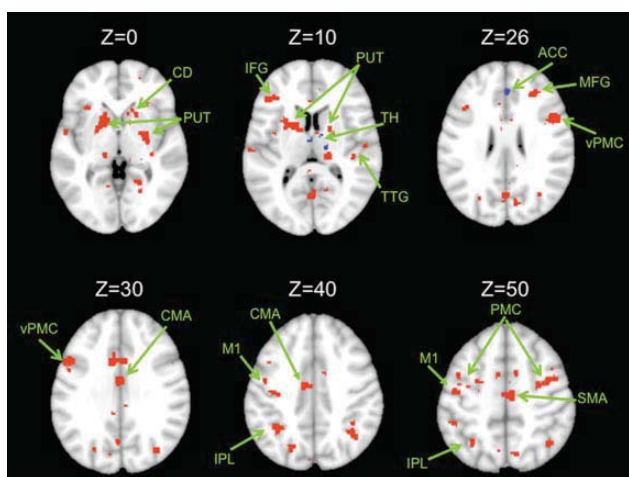
Figure 3. Connectivity maps in the whole brain. Functional connectivity maps for the dorsal (red) and ventral (blue) dentate seeds in the whole brain (axial views; both presented at $P < 0.00001$). The dorsal network consists primarily of motor and parietal regions, though there are also prefrontal regions included. The ventral network consists of the anterior cingulate cortex and the caudate. Images are oriented such that the right hemisphere is presented on the right. ACC, anterior cingulate cortex; CMA, cingulate motor area; CD, caudate; IPL, inferior parietal lobule; M1, primary motor cortex; MFG, middle frontal gyrus; PUT, putamen; SFG, superior frontal gyrus; TH, thalamus; TTG, transverse temporal gyrus; PMC, premotor cortex; d, dorsal; v, ventral. Unlabeled areas are extensions from the clusters presented in Table 2.

parietal lobule (Fig. 3; Table 2). The dorsal seed was also correlated with more anterior prefrontal regions including the inferior frontal gyrus, just anterior to the premotor cortex, as well as temporal lobe regions and the caudate. By contrast, the ventral dentate showed statistically significant connectivity with the anterior cingulate cortex, the caudate, and the thalamus (Fig. 3; Table 2).

Comparison of the Dorsal and Ventral Dentate Networks

To investigate the distinctiveness of these 2 dentate networks, we conducted a conjunction analysis. The results of this

Seed	Region	BA	MNI coordinates			T-value
			X	Y	Z	
Dorsal dentate	**Cerebellum**	–	12	−56	−30	11.44
	Brainstem	–	−16	−26	−4	10.07
	Cingulate motor area	24	−8	−10	40	9.64
	Inferior frontal gyrus/ventral premotor cortex	**9**	**44**	**4**	**20**	**9.68**
		9	54	10	26	8.70
	Dorsal premotor cortex	6	38	−4	48	8.25
	Angular gyrus	**39**	**36**	**−74**	**32**	**9.41**
	Middle temporal gyrus	39	34	−66	24	6.70
		19	36	−78	18	5.70
	Inferior parietal lobule	**40**	**−32**	**−44**	**32**	**8.91**
		40	−36	−52	44	8.12
	Precuneus	47	−20	−70	40	7.60
	Putamen	**–**	**−16**	**10**	**0**	**8.77**
			−22	2	2	8.53
	Caudate	–	−14	−6	16	7.96
	Primary motor cortex	**4**	**−38**	**−16**	**40**	**7.91**
			−44	−12	52	7.80
	Middle frontal gyrus	**9**	**30**	**36**	**22**	**7.90**
	Inferior frontal gyrus	46	50	30	16	7.49
	Superior frontal gyrus	9	24	42	36	6.76
	Inferior frontal gyrus	**47**	**28**	**28**	**2**	**6.97**
	Insula	–	38	16	2	5.99
	Inferior frontal gyrus	47	36	28	0	5.58
	Transverse temporal gyrus	**42**	**56**	**−14**	**10**	**6.96**
	Superior temporal gyrus	21	50	−22	2	6.86
	Transverse temporal gyrus	41	42	−26	10	6.79
	Superior frontal gyrus	**10**	**24**	**52**	**4**	**6.79**
	Inferior frontal gyrus	10	38	44	−4	6.68
	Middle frontal gyrus	10	32	56	−6	4.82
Ventral dentate	**Anterior cingulate cortex**	**24**	**−10**	**20**	**24**	**7.74**
		32	2	36	26	6.61
	Caudate	–	−12	10	20	6.11
	Thalamus	**–**	**2**	**−8**	**8**	**6.97**
	Thalamus ventral lateral nucleus	–	14	−16	10	6.69
	Caudate	–	20	−12	22	6.19

Negative x-values indicate locations in the left hemisphere, while positive x-values indicate locations in the right hemisphere. Regions in bold indicate the peak voxel of a cluster. Additional local maxima are presented in standard font. Cerebellar peaks are noted if there are cortical local maxima, but specific lobular locations are only included in Table 1 due to the cerebellar normalization procedures.

analysis are presented in Figure 4. Overall, there were very few areas of overlap between the 2 networks. When comparing the 2 networks in the cerebellum, we found overlap in lobule VI, as well as within the dentate itself (Fig. 4A). Our whole-brain investigation revealed overlap only in the anterior cingulate cortex (Fig. 4B). Thus, though there are some regions of overlap, these findings support a general dissociation between the dorsal and ventral dentate networks, particularly with respect to the primary motor, premotor, and prefrontal cortical regions.

Dorsal and Ventral Network Dissociability Using Cortical Seeds

To further investigate the dorsal and ventral dentate network distinction, we also placed seeds in several locations within the cortex. Here, we will focus on correlations with the dentate nucleus, but a complete list of correlated regions in the cerebellum is presented in Table 3. The seed placed in the primary motor cortex was correlated with the dorsal dentate nucleus, whereas the frontal pole seed was correlated with the ventral dentate nucleus. In both seeds, these were the only dentate correlations, further supporting the dissociability of the 2 networks. Notably however, the seed placed in the DLPFC was not correlated with the dentate nucleus, though there was connectivity in the area of the interposed nuclei.
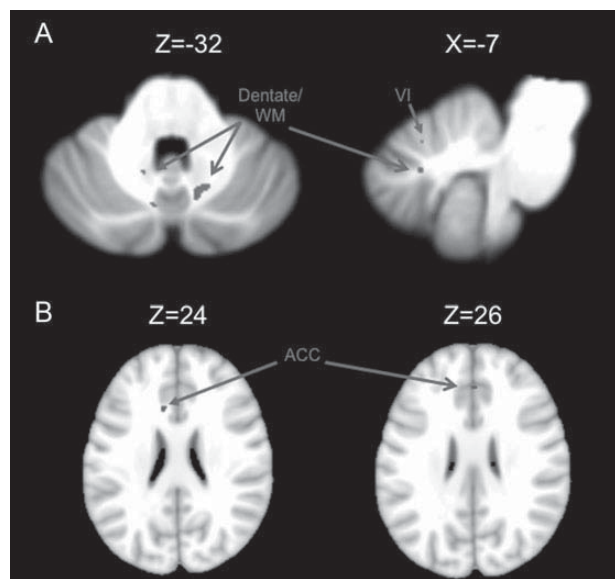
Figure 4. Regions of overlap in the dorsal and ventral networks. The results of our conjunction analysis indicative of overlap between the 2 networks are presented in, (*A*) the cerebellum, and (*B*). the whole brain. All images are oriented such that the right hemisphere is presented on the right. Roman numerals indicate the cerebellar lobules. ACC, anterior cingulate cortex.

Spatial Specificity of the Dorsal and Ventral Dentate Networks

In order to better understand the spatial specificity of the dorsal and ventral dentate networks, we placed additional seeds in the dorsal and ventral regions of the dentate nucleus (Supplementary Tables 1 and 2). The additional dorsal dentate seed (10, −58, −31), located more medially and ventral than our primary seed, was correlated with lobule V, crus II, and regions of the vermis and brainstem. In the cortex, correlated regions included the primary motor cortex, premotor regions, the inferior parietal lobule, precuneus, and regions of the temporal lobe. The additional ventral seed, located more laterally (20, −56, −37) with respect to our primary seed, was correlated with posterior regions of the cerebellum including crus I and lobule IX, but it was also correlated with lobules I–IV and VI. This additional ventral dentate seed was not however correlated with any additional regions in the whole brain.

Reproducibility of the Dorsal and Ventral Dentate Networks

We completed further post hoc analyses to examine the reproducibility of these networks in the nondominant hemisphere. We placed seeds in locations of the left dentate nucleus that mirrored the right side locations. The results of these analyses are presented in Supplementary Tables 3 and 4. The dorsal seeds were correlated primarily with more anterior regions of the cerebellum, though the first seed we tested was also correlated with crus I. In the whole brain, the correlations for both of these seeds included the anterior and posterior cingulate cortices, the precuneus, and prefrontal cortical regions. Many of the aspects of these networks are comparable to the default mode network. The ventral seeds in the left hemisphere are correlated primarily with lobules V and VI, though there are correlations with VIIb as well. Only the more lateral ventral seed (−20, −56, −37) shows correlations with the

whole brain. These results reveal a network that is largely consistent with the default mode network including the precuneus and posterior cingulate cortex.

Discussion

Our findings demonstrate that the dorsal and ventral dentate nucleus make up 2 distinct motor and cognitive networks, respectively, in the human brain. This distinction is particularly notable in the cerebral cortex. These networks are generally consistent with those identified in anatomical tract-tracing studies in nonhuman primates (Dum and Strick 2003) and, to our knowledge, provide the first demonstration of these distinct "networks" in the human brain. Similarities and differences between our findings and those in the animal literature are however examined in more detail below. Although we cannot assess directionality of these connections with fcMRI, our findings are in line with the idea of a closed loop system implying that distinct regions of the cerebellum are involved in processing information from distinct regions of the cortex.

Resting-state functional connectivity has proven to be a useful tool in the study of human cerebellar networks in vivo. Investigators have identified distinct motor and prefrontal networks of the cerebellar lobules in humans using this approach (Habas et al. 2009; Krienen and Buckner 2009; O'Reilly et al. 2010; Buckner et al. 2011; Bernard et al. 2012). Allen et al. (2005) demonstrated functional connectivity between the dentate nucleus and prefrontal and parietal regions of the cortex, though surprisingly little connectivity with motor cortical regions. We harnessed this technique to better understand the networks of the human dentate nucleus and our findings are similar to the dorsal and ventral networks mapped in nonhuman primates using invasive tract-tracing methods (Dum and Strick 2003).

Though our dorsal motor network did include prefrontal cortical regions, the general finding of dissociable networks within the dentate further supports models of cerebellar processing which posit its role in both motor and cognitive functions. Given the homogeneity of the cytoarchitecture of the cerebellum it has been proposed that cerebellar processing is consistent across its subregions (Ghez 1991; Ramnani 2006). Thach (1998) has proposed that the cerebellum links stimuli to their appropriate responses within a given context and that this may also apply to cognitive behaviors as well. Relatedly, both Ramnani (2006) and Ito (2008) have proposed models of cerebellar processing in the cognitive domain. Ramnani (2006) likens this processing to the forward model for motor control. An efference copy of the motor command is processed by the cerebellum and used to predict the expected sensory outcome of the movement. This prediction is then compared with the actual sensory consequences of the movement and the model is updated for future actions. Ramnani (2006) proposes that there may be similar efference copies of the processes computed in the prefrontal cortex undergoing comparable computations in the cerebellum. Ito (2008) has also proposed that the cerebellum processes internal models of the properties of mental activity in the cortex through either forward or inverse models. In all of these instances, distinct cerebellar–cortical networks are proposed to retain segregated processing. Our results further support the existence of segregated motor and cognitive networks in the dentate, in line with the notion that the cerebellum performs

Seed	Region	X	Y	Z	T-value
Primary motor cortex (−42, −24, 60	**Medulla**	**11**	**−23**	**3**	**8.85**
		12	−30	−1	6.88
		20	−28	−5	5.15
	Pons	**10**	**−28**	**−38**	**7.88**
	Pons	**−3**	**−30**	**−27**	**6.68**
		−10	−28	−31	6.11
		0	−25	−36	5.84
	Lobules I–IV	**20**	**−32**	**−19**	**6.43**
	Lobules I–IV	**−5**	**−51**	**−11**	**6.20**
	Vermis VIIIa	**5**	**−67**	**−42**	**6.12**
	Lobule IX/white matter	11	−57	−42	5.57
	Lobules I–IV	**−7**	**−43**	**−20**	**5.95**
	Medulla	**3**	**−29**	**−14**	**5.89**
	Lobule IX	**−7**	**−59**	**−43**	**5.86**
		−8	−51	−43	5.15
	Crus II	**10**	**−81**	**−36**	**5.83**
	Crus I	**50**	**−55**	**−28**	**5.81**
	Lobule VI	**−19**	**−66**	**−27**	**5.71**
	Lobule V	**9**	**−63**	**−18**	**5.57**
	Lobule VIIb	**41**	**−61**	**−52**	**5.48**
	Lobule V	**11**	**−56**	**−21**	**5.42**
	Lobule VI	**6**	**−62**	**−25**	**5.33**
	Lobule VI	**−23**	**−51**	**−27**	**4.45**
	Lobule I–IV	−9	−44	−26	5.10
	Lobule VI	**−10**	**−77**	**−22**	**5.24**
	Crus II	**−2**	**−78**	**−38**	**5.14**
	Lobule VIIIa	**−20**	**−61**	**−57**	**5.08**
	Lobule VIIIa	**0**	**−73**	**−40**	**5.05**
	Lobules I–IV	**−5**	**−44**	**−6**	**5.02**
	Dorsal dentate	**13**	**−62**	**−28**	**4.17**
	Lobule VIIb	**−8**	**−70**	**−44**	**4.88**
	Lobule VIIIb	**11**	**−61**	**−52**	**4.86**
	Crus II	**−10**	**−78**	**−36**	**4.85**
	Medulla	**4**	**−38**	**−10**	**4.84**
	Lobule VI	**23**	**−78**	**−21**	**4.84**
	Pons	**9**	**−26**	**−23**	**4.83**
DLPFC (−42, 16, 36)	**Lobule IX**	**8**	**−57**	**−39**	**6.55**
	Vermis IX	−1	−54	−34	7.52
	Lobule IX	6	−51	−44	6.80
	Pons	**13**	**−31**	**−11**	**9.64**
	Lobule V	5	−60	−11	9.03
	Crus I	**17**	**−80**	**−31**	**7.98**
	Crus II	8	−91	−30	7.78
	Crus I	21	−71	−35	7.06
	Lobule VI	**25**	**−62**	**−29**	**7.62**
		14	−66	−28	7.05
	Crus II	**−33**	**−68**	**−47**	**7.10**
	Crus II	**−19**	**−91**	**−36**	**6.95**
		−11	−78	−33	6.80
		−6	−84	−31	6.32
	Midbrain	**3**	**−30**	**−16**	**6.91**
	Lobule VI	**−23**	**−61**	**−29**	**6.60**
		−16	−66	−30	4.85
	Crus II	**−41**	**−57**	**−46**	**6.58**
	Crus I	**−37**	**−64**	**−27**	**6.44**
	Crus I	**41**	**−72**	**−23**	**6.03**
	Lobule VI	**34**	**−64**	**−21**	**5.99**
	Lobule V	**−17**	**−52**	**−27**	**5.98**
	Lobule IX	**−7**	**−51**	**−42**	**5.79**
	Vermis VI	**−5**	**−68**	**−19**	**5.60**
	Crus II	**35**	**−78**	**−49**	**5.44**
	Lobule V	**−20**	**−44**	**−20**	**5.43**
	Vermis crus II	**0**	**−73**	**−38**	**5.32**
	Lobule VI	**−19**	**−60**	**−14**	**5.30**
	Crus II	**8**	**−83**	**−41**	**5.30**
	Lobule VIIb	**37**	**−64**	**−49**	**5.24**
	Interposed nuclei	**12**	**−48**	**−32**	**5.22**
	Crus I	**20**	**−90**	**−25**	**5.16**
	Vermis crus II	**2**	**−71**	**−33**	**5.15**
	Crus II	**−36**	**−74**	**−55**	**5.14**
	Vermis VIIIa	**1**	**−72**	**−43**	**5.11**
	Crus I	**27**	**−71**	**−29**	**5.10**
	Lobule VIIb	**−7**	**−71**	**−37**	**5.10**
	Lobule VI	**35**	**−41**	**−41**	**5.08**

(continued)

Seed	Region	MNI coordinates			T-value
		X	Y	Z	
	Crus II	**41**	**−74**	**−46**	**5.08**
	Crus I	**38**	**−75**	**−23**	**5.06**
	Pons	**2**	**−32**	**−25**	**5.04**
	Lobule VI	**−5**	**−73**	**−12**	**5.04**
	Lobule VI	**−13**	**−72**	**−29**	**4.93**
	Crus I	**−36**	**−53**	**−35**	**4.93**
	Lobule VIIIb	**−20**	**−57**	**−59**	**4.92**
	Lobule VIIIa	**−29**	**−37**	**−45**	**4.86**
	Lobule VIIb	**28**	**−67**	**−55**	**4.86**
	Crus I	**33**	**−86**	**−34**	**4.74**
	Lobules I–IV	**−6**	**−45**	**−6**	**4.73**
	Midbrain	**8**	**−32**	**−12**	**4.73**
	Lobule V	**20**	**−42**	**−14**	**4.65**
	Lobule VI	**−14**	**−66**	**−21**	**4.64**
	Lobule VI	**−25**	**−43**	**−31**	**4.63**
Frontal pole (0, 62, 4)	**Lobule IX**	**7**	**−56**	**−38**	**10.46**
	Crus I	−22	−77	−36	9.52
	Crus I	**−34**	**−55**	**−34**	**7.08**
		−44	−64	−34	5.49
		−46	−61	−43	5.33
	Crus II	**−38**	**−66**	**−46**	**6.49**
		−40	−72	−55	5.64
	Medulla	**5**	**−23**	**−15**	**4.95**
	Crus I	**−51**	**−75**	**−39**	**4.75**
	Ventral dentate nucleus	**−25**	**−52**	**−42**	**4.69**
	Lobule VIIIb	**17**	**−44**	**−58**	**4.64**
	Crus I	**−44**	**−58**	**−27**	**4.57**
	Crus II	**−18**	**−83**	**−43**	**4.55**
	Lobule VIIIa	**22**	**−60**	**−55**	**4.49**
	Lobule X	**36**	**−32**	**−45**	**4.48**
	Crus I	**−49**	**−71**	**−42**	**4.46**
	Crus II	**−36**	**−75**	**−48**	**4.44**
	Lobule VIIIa	**30**	**−49**	**−58**	**4.42**
	Lobule VIIb	**−9**	**−70**	**−42**	**4.34**

All results are corrected using at FDR $P < 0.001$ and each cluster is a minimum of 10 voxels. Negative x-values indicate locations in the left hemisphere, while positive x-values indicate locations in the right hemisphere. Regions in bold indicate the peak voxel of a cluster. Additional local maxima are presented in standard font.

similar information processing but on distinct inputs, which results in distinct outputs to the cortex.

Significant overlap based on our conjunction analysis was demonstrated in the dentate nucleus, and lobule VI. Within the dentate nucleus, this is likely due to correlations with each seed region with itself, extending into this intermediate region. Regarding lobule VI, it may indeed subserve both motor and cognitive functions; functional neuroimaging studies have demonstrated activation in lobule VI during working memory performance (Chen and Desmond 2005a, 2005b; Stoodley et al. 2012) while a meta-analysis has also indicated a role for this lobule in motor tasks (Stoodley and Schmahmann 2009). Recent neuroimaging work has demonstrated a homunculus representation within lobule VI that is relevant to the performance of complex motor tasks (Schlerf et al. 2010), and related activity was also seen in crus I.

The conjunction analysis in the whole brain revealed overlap only in the anterior cingulate cortex (ACC). The overlap in the ACC may also be due to multimodal processing in this region. There are regions of the ACC associated with motor processing (Picard and Strick 1996), and an event-related potential associated with the region has been linked to processing of motor errors (Anguera et al. 2009). In general, the lack of overlap between the 2 dentate networks supports their general dissociability.

Overall, it may be that the partially overlapping dorsal and ventral dentate networks that we observed within the cerebellum and whole brain are due to involvement of some of these regions in both motor and cognitive processing. Additionally, the correlations with the seeds themselves extended into an intermediate region of the dentate nucleus. This may also be contributing in part to the overlap seen in our conjunction analysis. We would stress however, that overall there is little overlap between the 2 networks, and we do not believe the existence of this overlap undermines the notion that these networks are largely dissociable.

In the dentate seeds of the left hemisphere, the correlations with the whole brain were limited to the dorsal seeds and the more lateral ventral seed. In general, these seeds were correlated with regions typically associated with the default mode network (Buckner et al. 2008), with some additional correlations with prefrontal cortex. In this case, all of our participants were right handed, meaning the right cerebellar hemisphere is dominant for motor functions. The dominance of the right cerebellum for motor tasks involving the dominant hand may result in a stronger dissociation between the motor and nonmotor functional networks of the right dentate nucleus. With greater use for motor tasks, these networks may become more specific in their targets for their given function. This may therefore underlie the lack of motor cortical correlations in the dorsal seeds of the left hemisphere, and the correlations with regions of the default mode network. Future studies would benefit from comparing the resting-state networks of the cerebellum in the dominant and nondominant hemispheres of left and mixed-handed individuals. Additionally, there may be anatomical asymmetries in the dentate nucleus across the 2 hemispheres. This too could result in the differing networks across the 2 hemispheres, and future studies would benefit from investigating this further.

We observed that the dorsal dentate exhibited correlated activity with the putamen. This is consistent with the nonhuman primate literature indicating that both the dorsal and ventral portions of the dentate are linked to the striatum (Hoshi et al. 2005). More recently, it has been demonstrated that the subthalamic nucleus of the basal ganglia has projections to the cerebellar cortex allowing for bidirectional communication loops between these 2 structures (Bostan et al. 2010). Though directionality cannot be assessed using fcMRI, we provide evidence supporting the potential for such processing loops in the human brain as well. The putamen is known to be part of a reciprocal circuit involving motor and premotor cortical areas while the caudate nucleus circuitry includes dorsolateral prefrontal cortex (Alexander and DeLong 1985a, 1985b; Alexander et al. 1986; Alexander and Crutcher 1990). Thus, connectivity between the dorsal dentate and putamen further fits with the interpretation of the dorsal dentate loop supporting motor functions.

The spatial specificity of the dorsal and ventral dentate networks was investigated, given the appearance of distinct regions which project to the prefrontal and motor cortex (Dum and Strick 2003). Our additional motor seed, located more ventral with respect to our primary seed, was also correlated primarily with premotor and primary motor regions, as well as the inferior parietal lobule and regions of the temporal lobe. This provides some indication of the extent of the motor region of the dentate nucleus, though

future studies with higher spatial resolution are needed to further investigate this. Notably, we did not see any topography within the primary motor cortex in our dorsal dentate seeds. While recent work has supported the notion of motor topography within the cerebellum (Buckner et al. 2011), and the dentate nucleus itself (Küper et al. 2012), there is still quite a bit of overlap between the different representations within the dentate. Thus, it would be difficult to see a similar somatotopy in our resting-state networks. Indeed, further studies with additional seeds and higher spatial resolution are warranted.

Of the 2 ventral seeds investigated, our main seed showed projections to the anterior cingulate cortex while our additional seed did not show any correlations outside of the cerebellum. The lack of correlations in the right hemisphere for our secondary ventral dentate seed are unexpected, particularly given that a seed placed in the mirrored location of the left hemisphere did show correlations with the whole brain. This further supports the notion of asymmetries between the hemispheres, and future work with higher spatial resolution is needed to further investigate potential topographic subregions in the ventral dentate nucleus.

While our results are generally consistent with the animal literature demonstrating that the dorsal dentate is part of a more motor network, and the ventral dentate is part of a cognitive network (Dum and Strick 2003), there were some surprising results across both the cerebellum and the cerebral cortex. Most notably, we did not demonstrate a correlation between the dorsal dentate nucleus of the right hemisphere and lobules VIIIa and VIIIb which are thought to serve motor functions (though this correlation was present in our left hemisphere seeds). Tract tracing in nonhuman primates has shown connections between the primary motor cortex and lobules VIIIa and VIIIb (Dum and Strick 2003), and they are associated with motor functions (Stoodley and Schmahmann 2009). However, the precise function of this posterior motor representation is unknown. It is thought to be different from that of the anterior motor representation, and is thought to be less important for motor control (Donchin et al. 2012). Therefore, we might expect to see a correlation between the dentate and this region in the cerebellum, but not necessarily in the same region that is correlated with the anterior lobules. Though we did investigate an additional seed in the right dorsal dentate nucleus, it may be an uninvestigated region that is correlated with the posterior motor area in lobules VIIIa and VIIIb. Furthermore, it is notable that within the cerebellum there were correlations between the dorsal seed and more posterior cognitive regions of the cerebellum, as well as correlations between the ventral seed and more anterior motor regions of the cerebellum. While this does indeed differ from the dissociation seen when investigating motor and prefrontal regions of the cortex in nonhuman primates (Kelly and Strick 2003), it is crucial to note that the resting-state approach is markedly different from that used in tract tracing. These anomalies may be due to some overlapping and similar cortical targets of the dentate seeds, as connectivity in the cerebellum is likely due to cortical activity given the anatomy and closed loop circuitry of the cerebellum. Thus while we did observe some mixing between the 2 networks in the cerebellum, this is not entirely surprising, nor does it undermine the general dissociation between the dorsal and ventral dentate networks.

With respect to the cortex, there are 2 key points worth noting. First, our dorsal seed did include some prefrontal areas, though they were distinct from the ACC, which was correlated with the ventral dentate. This differs from findings in the animal literature (Dum and Strick 2003; Kelly and Strick 2003), but may reflect at least in part, the morphological differences between the dentate nucleus and cerebellum more generally in humans and nonhuman primates (Leiner et al. 1986, 1993; Balsters et al. 2009). These cortical regions were typically adjacent to the premotor regions and may also reflect similarities in the resting-state signal between premotor and more prefrontal cognitive regions. Thus, while the dorsal dentate networks are not solely motor, the additional regions involved may be due to their proximity to those needed for motor processing. Furthermore, despite these prefrontal components, the dorsal and ventral dentate networks are indeed distinct in their cortical components. Second, while the networks are largely lateralized to the left hemisphere (for right hemisphere seeds) there are some correlations ipsilateral to the dentate seed. This was somewhat unexpected; however, this is likely due to the bilateral correlations within the cerebellum itself at rest.

Conclusions

Our data demonstrate that the human dentate nucleus is part of 2 distinct functional networks. These networks are associated with topographically unique regions of the dentate nucleus, roughly spatially consistent with findings from nonhuman primates (Dum and Strick 2003). The dorsal dentate is part of a network that includes anterior regions of the cerebellum, as well as primary motor and premotor cortex. The ventral dentate is part of a network that includes posterior regions of the cerebellum, known to evolve in conjunction with the prefrontal cortex (Balsters et al. 2009), and regions of the anterior prefrontal cortex associated with higher cognitive functions. To our knowledge, this is the first study to dissociate 2 functional networks within the human dentate nucleus dedicated to motor and cognitive processing.

Supplementary Material

Supplementary material can be found at: http://www.cercor.oxford-journals.org/.

References

Akkal D, Dum RP, Strick PL. 2007. Supplementary motor area and presupplementary motor area: targets of basal ganglia and cerebellar output. J Neurosci. 27:10659–10673.

Alexander GE, Crutcher MD. 1990. Functional architecture of basal ganglia circuits: neural substrates of parallel processing. Trends Neurosci. 13:266–271.

Alexander GE, DeLong MR. 1985a. Microstimulation of the primate neostriatum: I. Physiological properties of striatal microexcitable zones. J Neurophysiol. 53:1417–1432.

Alexander GE, DeLong MR. 1985b. Microstimulation of the primate neostriatum: II. Somatotopic organization of striatal microexcitable zones and their relation to neuronal response properties. J Neurophysiol. 53:1433–1446.

Alexander GE, DeLong MR, Strick PL. 1986. Parallel organization of functionally segregated circuits linking basal ganglia and cortex. Annu Rev Neurosci. 9:357–381.

Allen G, McColl R, Barnard H, Ringe WK, Fleckenstein J, Cullum CM. 2005. Magnetic resonance imaging of cerebellar-prefrontal and cerebellar-parietal functional connectivity. NeuroImage. 28:39–48.

Anguera JA, Seidler RD, Ghering WJ. 2009. Changes in performance monitoring during sensorimotor adaptation. J Neurophysiol. 102:1868–1879.

Balsters JH, Cussans E, Diedrichsen J, Phillips KA, Preuss TM, Rilling JK, Ramnani N. 2009. Evolution of the cerebellar cortex: the selective expansion of prefrontal-projecting cerebellar lobules. NeuroImage. 49:2045–2052.

Bernard JA, Seidler RD, Hassevoort KM, Benson BL, Welsh RC, Wiggins JL, Jaeggi SM, Buschkuehl M, Monk CS, Jonides J et al. 2012. Resting state cortico-cerebellar functional connectivity networks: a comparison of anatomical and self-organizing map approaches. Front Neuroanat. 6:31.

Biswal B, Mennes M, Zuo X-N, Gohel S, Kelly C, Smith SM, Beckman CF, Adelstein JS, Buckner RL, Colcombe S et al. 2010. Toward discovery science of human brain function. Proc Nat Acad Sci USA. 107:4734–4739.

Biswal B, Yetkin FZ, Haughton VM, Hyde JS. 1995. Functional connectivity in the motor cortex of resting human brain using echoplanar MRI. Magn Reson Med. 34:537–541.

Bostan AC, Dum RP, Strick PL. 2010. The basal ganglia communication with the cerebellum. Proc Nat Acad Sci USA. 107:8452–8456.

Buckner RL, Andrews-Hanna JR, Schacter DL. 2008. The brain's default network: anatomy, function, and relevance to disease. Ann NY Acad Sci. 1124:1–38.

Buckner RL, Krienen FM, Castellanos A, Diaz JC, Yeo BT. 2011. The organization of the human cerebellum estimated by intrinsic functional connectivity. J Neurophys. 106:2322. –2245.

Chen SHA, Desmond JE. 2005b. Cerebrocerebellar networks during articulatory rehearsal and verbal working memory tasks. NeuroImage. 24:332–338.

Chen SHA, Desmond JE. 2005a. Temporal dynamics of cerebro-cerebellar network recruitment during a cognitive task. Neuropsychologia. 43:1227–1237.

Clower DM, Dum RP, Strick PL. 2005. Basal ganglia and cerebellar inputs to "AIP". Cereb Cortex. 15:913–920.

Desmond JE, Chen SHA, Shieh PB. 2005. Cerebellar transcranial magnetic stimulation impairs verbal working memory. Ann Neurol. 8:53–560.

Diedrichsen J. 2006. A spatially unbiased atlas template of the human cerebellum. NeuroImage. 33:127–138.

Diedrichsen J, Balsters JH, Flavell J, Cussans E, Ramnani N. 2009. A probabilistic MR atlas of the human cerebellum. NeuroImage. 46:39–46.

Diedrichsen J, Maderwald S, Küper M, Thurling M, Rabe K, Gizewski ER, Ladd ME, Timmann D. 2011. Imaging the deep cerebellar nuclei: a probabilistic atlas and normalization procedure. NeuroImage. 54:1786–1794.

Diedrichsen J, Verstynen T, Schlerf J, Wiestler T. 2010. Advances in functional neuroimaging of the human cerebellum. Curr Opin Neurol. 23:382–387.

Dimitrova A, Weber J, Redies C, Kindsvater K, Maschke M, Kolb FP, Forsting M, Diener HC, Timmann D. 2002. MRI atlas of the human cerebellar nuclei. NeuroImage. 17:240–255.

Donchin O, Rabe K, Diedrichsen J, Lally N, Schoch B, Gizewski ER, Timmann D. 2012. Cerebellar regions involved in adaptation to force field and visuomotor perturbation. J Neurophysiol. 107:134–147.

Dum RP, Strick PL. 2003. An unfolded map of the cerebellar dentate nucleus and its projections to the cerebral cortex. J Neurophysiol. 89:634–639.

Ghez C. 1991. The cerebellum. In: Kandel ER, Schwartz JH, Jessell TM, editors. Principles of neural science. Norwalk (CT): Appleton & Lange. p. 626–646.

Gilbert SJ, Simons JS, Frith CD, Burgess PW. 2006. Performance-related activity in medial rostral prefrontal cortex (area 10) during low-demand tasks. J Exp Psychol Hum. 32:45–58.

Glickstein M, Doron K. 2008. Cerebellum: connections and functions. Cerebellum. 7:589–594.

Glover GH, Law CS. 2001. Spiral-in/out BOLD fMRI for increased SNR and reduced susceptibility artifacts. Magn Reson Med. 46:515–522.

Glover GH, Li TQ, Ress D. 2000. Image-based method for retrospective correction of physiological motion effects in fMRI:RETROICOR. Magn Reson Med. 44:162–167.

Gusnard DA, Raichle ME. 2001. Searching for a baseline: functional imaging and the resting human brain. Nat Rev Neurosci. 2:685–694.

Habas C. 2010. Functional imaging of the deep cerebellar nuclei: a review. Cerebellum. 9:22–28.

Habas C, Kamdar N, Nguyen D, Prater K, Beckmann CF, Menon V, Greicius MD. 2009. Distinct cerebellar contributions to intrinsic connectivity networks. J Neurosci. 29:8586–8594.

Hoshi E, Tremblay L, Féger J, Carras P, Strick PL. 2005. The cerebellum communicates with the basal ganglia. Nat Neurosci. 8:1491–1493.

Ito M. 2008. Control of mental activities by internal models in the cerebellum. Nat Rev Neurosci. 9:304–313.

Jenkinson M, Banniseter P, Brady M, Smith S. 2002. Improved optimization for the robust and accurate linear registration and motion correction of brain images. NeuroImage. 17:825–841.

Kelly RM, Strick PL. 2003. Cerebellar loops with motor cortex and prefrontal cortex of a nonhuman primate. J Neurosci. 23:8432–8444.

Kim S-G, Ugurbil K, Strick PL. 1994. Activation of a cerebellar output nucleus during cognitive processing. Science. 265:949–951.

Krienen FM, Buckner RL. 2009. Segregated fronto-cerebellar circuits revealed by intrinsic functional connectivity. Cereb Cortex. 19:2485–2497.

Küper M, Dimitrova A, Thürling M, Maderwald S, Roths J, Elles HG, Gizewski ER, Ladd ME, Diedrichsen J, Timmann D. 2011. Evidence for a motor and a non-motor domain in the human dentate nucleus—an fMRI study. NeuroImage. 54:2612–2622.

Küper M, Thürling M, Stefansecu R, Maderwald S, Roths J, Elles HG, Ladd ME, Diedrichsen J, Timmann D. 2012. Evidence for a motor somatotopy in the cerebellar dentate nucleus—an fMRI study in humans. Hum Brain Mapp. 33:2741–2749.

Leiner HC, Leiner AL, Dow RS. 1993. Cognitive and language functions of the human cerebellum. Trends Neurosci. 16:444–447.

Leiner HC, Leiner AL, Dow RS. 1986. Does the cerebellum contribute to mental skills? Behav Neurosci. 100:443–454.

Middleton FA, Strick PL. 2001. Cerebellar projections to the prefrontal cortex of the primate. J Neurosci. 21:700–712.

Oppenheim A, Schafer R, Buck J. 1999. Discrete-time signal processing. Upper Saddle River (NJ): Prentice Hall.

O'Reilly JX, Beckmann CF, Tomassini V, Ramnani N, Johansen-Berg H. 2010. Distinct and overlapping functional zones in the cerebellum defined by resting state functional connectivity. Cereb Cortex. 20:953–965.

Peltier SJ, Polk TA, Noll DC. 2003. Detecting low-frequency functional connectivity in fMRI using a self-organizing map (SOM) algorithm. Hum Brain Mapp. 20:220–226.

Picard N, Strick PL. 1996. Motor areas of the medial wall: a review of their location and functional activation. Cereb Cortex. 6:342–353.

Ramnani N. 2006. The primate cortico-cerebellar system: anatomy and function. Nat Rev Neurosci. 7:511–522.

Schlerf JE, Verstynen TD, Ivry RB, Spencer RMC. 2010. Evidence of a novel somatopic map in the human neocerebellum during complex actions. J Neurophysiol. 103:3330–3336.

Schmahmann JD, MacMore J, Vangel M. 2009. Cerebellar stroke without motor deficit: clinical evidence for motor and non-motor domains within the human cerebellum. Neuroscience. 162:852–861.

Stoodley CJ, Schmahmann JD. 2009. Functional topography in the human cerebellum: a meta-analysis of neuroimaging studies. NeuroImage. 44:489–501.

Stoodley CJ, Valera EM, Schmahmann JD. 2012. Functional topography of the cerebellum for motor and cognitive tasks: an fMRI study. NeuroImage. 59:1560–1570.

Strick PL, Dum RP, Fiez JA. 2009. Cerebellum and nonmotor function. Annu Rev Neurosci. 32:413–434.

Thach WT. 1998. What is the role of the cerebellum in motor learning and cognition? Trends Cogn Sci. 2:331–337.

Thürling M, Küper M, Stefanescu R, Maderwald S, Gizewski ER, Ladd ME, Timmann D. 2011. Activation of the dentate nucleus in a verb generation task: a 7T MRI study. NeuroImage. 57:1184–1191.